Camera traps enable the estimation of herbaceous aboveground net primary production (ANPP) in an African savanna at high temporal resolution

de Jonge, Inger K.; Veldhuis, Michiel P.; Vrieling, Anton; Olff, Han

Published in:
Remote Sensing in Ecology and Conservation

DOI:
10.1002/rse2.263

Remote Sensing in Ecology and Conservation
Open Access
ZSL LET'S WORK FOR WILDLIFE

ORIGINAL RESEARCH

Camera traps enable the estimation of herbaceous aboveground net primary production (ANPP) in an African savanna at high temporal resolution

Inger K. de Jonge[1,2], Michiel P. Veldhuis[3], Anton Vrieling[4] & Han Olff[1]

[1]Conservation Ecology, Groningen Institute for Evolutionary Life Sciences, University of Groningen, P.O. Box 11103, Groningen NL-9700 CC, The Netherlands
[2]Department of Ecological Science, Systems Ecology, Faculty of Science, Vrije Universiteit Amsterdam, De Boelelaan 1085, Amsterdam 1081 HV, The Netherlands
[3]Department of Environmental Biology, Institute of Environmental Sciences, Leiden University, Einsteinweg 2, Leiden 2333 CC, The Netherlands
[4]Faculty of Geo-information Science and Earth Observation, University of Twente, P.O. Box 217, Enschede 7500 AE, The Netherlands

Keywords
ANPP, digital repeat photography, grasslands, rangelands, remote sensing, Sentinel-2

Correspondence
Inger K. de Jonge, Department of Ecological Science, Systems Ecology, Faculty of Science, Vrije Universiteit Amsterdam, De Boelelaan 1085, 1081 HV Amsterdam, The Netherlands. Tel: +31 20 59 84254, E-mail: ingerdejonge@gmail.com

Editor: Marcus Rowcliffe
Associate Editor: Dolors Armenteras

Received: 29 July 2021; Revised: 18 February 2022; Accepted: 4 March 2022

doi: 10.1002/rse2.263

Remote Sensing in Ecology and Conservation 2022;**8** (5):583–600

Abstract

Determining the drivers of aboveground net primary production (ANPP), a key ecosystem process, is an important goal of ecosystem ecology. However, accurate estimation of ANPP across larger areas remains challenging, especially for savanna ecosystems that are characterized by large spatiotemporal heterogeneity in ANPP. Satellite remote sensing methods are frequently used to estimate productivity at the landscape scale but generally lack the spatial and temporal resolution to capture the determinants of productivity variation. Here, we developed and tested methods for estimating herbaceous productivity as an alternative to labour-intensive repeated biomass clipping and caging of small plots. We compared measures of three spectral greenness indices, normalized difference vegetation index derived from Sentinel-2 (NDVIs) and a handheld radiometer (NDVIg), and green chromatic coordinate derived from digital repeat cameras (GCC) and tested their relationship to biweekly field-measured herbaceous ANPP using movable exclosures. We found that a satellite-based model including average NDVIs and its rate of change (ΔNDVIs) over the biweekly productivity measurement interval predicted herbaceous ANPP reasonably well (Jackknife $R^2 = 0.26$). However, the predictive accuracy doubled (Jackknife $R^2 = 0.52$) when including the sum of day to day increases in camera trap-derived vegetation greenness (tGCC). This result can be considered promising, given the current lack of productivity estimation methods at comparable spatiotemporal resolution. We furthermore found that the fine (daily) temporal resolution of GCC time series captured fast vegetation responses to rainfall events that were missed when using a coarser temporal resolution (>2 days). These findings demonstrate the importance of measuring at a fine temporal resolution for predicting herbaceous ANPP in savanna ecosystems. We conclude that camera traps are promising in offering a reliable and cost-effective method to estimate productivity in savannas and contribute to a better understanding of ecosystem functioning and its drivers.

Introduction

Aboveground net primary production (ANPP) is considered a key aspect of ecosystem functioning because of its defining influence on ecosystem structure and biological diversity (Brun et al., 2019; Cebrian, 1999; McNaughton et al., 1989). Determining the causes of spatial and temporal variation in ANPP is, therefore, an important goal in ecosystem ecology, including the assessment of ecosystem services (Reid et al., 2006). The accurate

measurement and estimation of ANPP at spatial and temporal resolutions that capture the relevant determinants of productivity in natural ecosystems remain challenging, especially in tropical savanna ecosystems due to their inherent high level of intra-annual rainfall variability, both in the amount, intensity and intermittency. Short-term changes in ANPP in response to stochastic rainfall events are likely to be missed because cloud cover during the rainy season can prevent optical satellite sensors from acquiring cloud-free imagery, thereby limiting the assessment of vegetation productivity at critical moments (Pettorelli et al., 2005). In addition, different ANPP estimation methods can produce inconsistent results due to ignoring the effects of grazing (extra production may rapidly be removed), turnover rates and decomposition in ANPP estimates (Ruppert & Linstädter, 2014; Scurlock et al., 2002). To better understand the functioning of savanna ecosystems, it is crucial to improve and develop methods for efficient estimation of ANPP at relevant scales while using 'best practice' methods as benchmarks to evaluate these estimation methods (Ruppert & Linstädter, 2014).

Traditionally, ANPP is estimated in the field using either clipping of peak standing biomass at the end of the growing season (so-called 'peak methods') or repeated clipping throughout the season ('incremental methods') (Byrne et al., 2011; Mbow et al., 2013). The majority of field-based herbaceous ANPP estimation methods rely on the less labour-intensive peak methods, but these are inadequate in savannas as these are fast turnover ecosystems with high ANPP to biomass ratios (Sala & Austin, 2000). Grazers can also affect productivity in multiple ways, *for example* by inducing compensatory growth in response to defoliation (Frank & McNaughton, 1993) and by reducing leaf area, reducing photosynthetic capacity. Therefore, the use of incremental methods in combination with moveable exclosures is preferred in natural savanna ecosystems (McNaughton et al., 1996). Despite the advantage of relatively accurate ANPP measurements that are possible through repeated caging and clipping, the high labour intensity limits its applicability. Therefore, to obtain accurate ANPP estimates for larger areas, such labour-intensive best-practice methods need to be calibrated to more rapid-assessment methods.

The increasing availability of multispectral satellite imagery makes satellite-derived vegetation indices (VI's), such as the Normalized Difference Vegetation Index (NDVI), a good candidate for such calibrations. Indeed, many ecological studies use NDVI as a proxy for vegetation productivity and phenology (Bonenfant et al., 2009; Paruelo et al., 1997; Pettorelli et al., 2011). At the basis of this relationship is the capability of NDVI to capture the contrast between strong absorption in the visible wavelengths and high reflectance in the near-infrared wavelengths, which characterizes photosynthetically active vegetation (Tucker, 1979). Important limitations of NDVI include its sensitivity to optical properties of the soil background (Huete et al., 1985), the quick saturation with increasing leaf area index (Baret & Guyot, 1991) and reduced temporal observations by satellites due to cloudiness (Pettorelli et al., 2005). Satellite-derived time series of NDVI with relatively short intervals between consecutive observations were until recently limited to spatial resolutions of c. 250–1000 m. One important example is the Moderate Resolution Imaging Spectroradiometer (MODIS) that flies on the Terra and Aqua satellites. In recent years, the revisit frequency has increased for freely available satellite data at finer spatial resolutions. For example, since the launch of the second Sentinel-2 satellite in March 2017, the mission now offers global coverage at 10 m resolution every 5 days. However, due to cloud cover, particularly an issue during rainy seasons (the main growing season), no frequent observations of the land surface can be made everywhere, thus limiting its potential to capture short-term vegetation responses to rain events. This is relevant as vegetation responses to rain occur rapidly in semi-arid ecosystems, especially for grasses (Williams et al., 1998; Xu et al., 2015). Methods that are only based on satellite-derived NDVI may therefore not fully capture temporal patterns of primary production, despite their excellent spatial coverage.

The use of digital repeat photography or 'near-surface remote sensing' in the study of phenology is gaining popularity across various ecosystems (Alberton et al., 2017; Richardson, 2019; Toomey et al., 2015; Vrieling et al., 2018). The resulting image series, obtained from digital cameras installed at a fixed position, allow for the derivation of greenness indicators such as the green chromatic coordinate (GCC), which expresses green reflection as a fraction of the total reflection in the visible spectrum for vegetation within the camera field-of-view (Richardson et al., 2013; Sonnentag et al., 2012). Given that the cameras can be set to take multiple images per day, they provide a method that is relatively insensitive to cloud cover. Digital repeat photography, possible with weather-proof, relatively cheap camera traps, can thus potentially capture fast vegetation responses to rain events. Unlike NDVI, absolute measures of GCC are less suitable for the estimation of biomass as the typical (and most practical in areas with wildlife due to the risk of damage) oblique mode of camera installation means that the GCC signal is affected by non-photosynthetic parts, such as flowers and seeds (Vrieling et al., 2018).

Although digital repeat photography has proven its usefulness for phenology studies (Vrieling et al., 2018), to the best of our knowledge, no attempts exist to use time

series of field photographs for estimating high-resolution ANPP. In this study, we compared temporal and integrated measures of two VI's (NDVI and GCC) derived from remote and near-surface sensing techniques and investigated their relationship with field-measured herbaceous ANPP using movable exclosures. Specifically, we examined the capacity of different combinations of sensing techniques, VI measures and a field-measured proxy for aboveground standing biomass to predict short-term (14 days) herbaceous ANPP. Last, we explored the spatiotemporal responsiveness of GCC to rainfall events and assessed how the predictive capacity of VI measures and field-measured biomass for ANPP was affected by a reduction in both temporal and spatial resolution.

Materials and Methods

Study area and design

The study was conducted around Seronera in the centre of the Serengeti National Park (SNP), North-western Tanzania (Fig. 1). The SNP is part of the greater Serengeti-Mara ecosystem, one of the largest protected tropical savanna ecosystems globally and home to abundant and diverse wildlife (Sinclair et al., 2008). The mean annual precipitation for Seronera is around 800 mm (Pellew, 1983). Rainfall is highly stochastic, both in intensity and intermittency, but annual rainfall generally peaks during the short rain season in December–January and during the long rain season in March–May. Seronera is situated at the fringe of the Serengeti plains and is characterized by gently rolling pediplains on granitic rocks (Jager, 1982). The vegetation is classified as Acacia woodlands, which is characterized by a continuous C4-grass dominated herbaceous layer (principal grass species include *Themeda triandra*, *Digitaria macroblephara* and *Panicum coloratum*) intermixed with a discontinuous layer of (predominantly *Vachellia tortilis and V. robusta*) trees.

We set up cameras in the vicinity of the research station in Seronera over two study periods (April–June 2016 and April–September 2018) (Fig. 1, see Table S1 for coordinates). Taking advantage of the 5-day temporal resolution of the Sentinel-2 multispectral instrument data since 2017, we set up a network of eight cameras (A–H) in April 2018. For these sites, we evaluated how both camera-derived GCC and Sentinel-2 derived NDVI (NDVIs) related to herbaceous ANPP. However, we had initiated the study in 2016 with two cameras (I–J), for which we solely evaluated the relationship between camera-derived GCC and herbaceous ANPP. We also measured NDVI on the ground (NDVIg) with a handheld radiometer every 4 days to compare the predictive capacities of GCC and NDVI without being dependent on

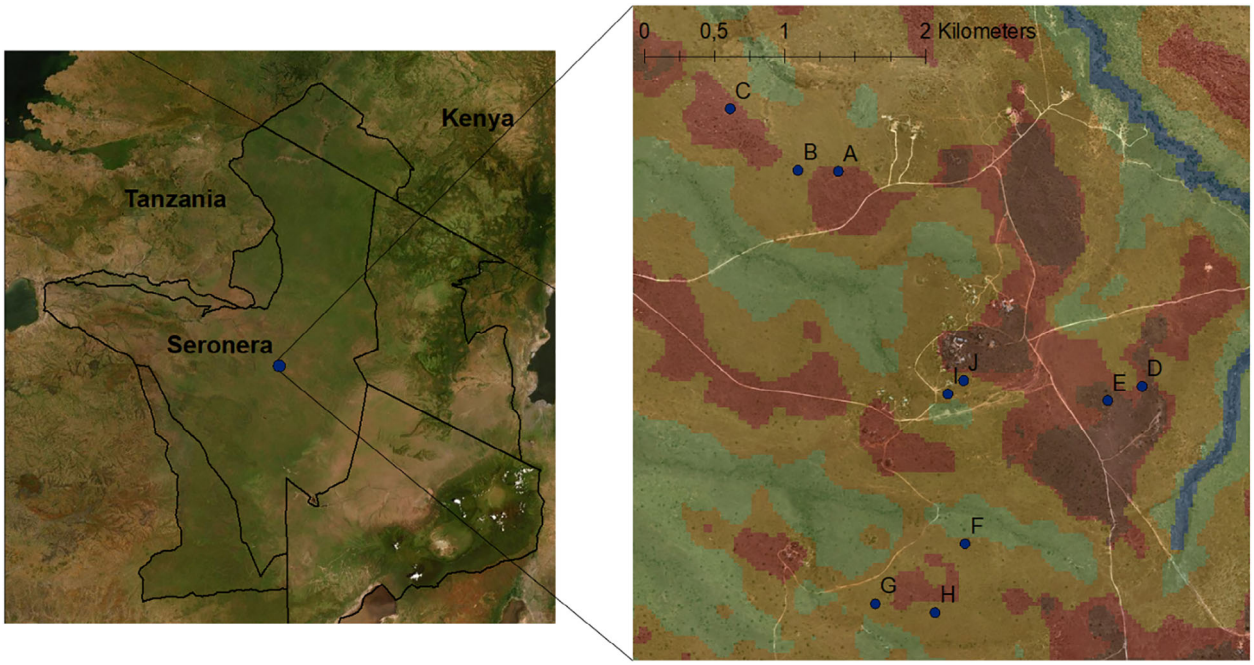

Figure 1. Study area and location of sites (A–J) across a topographical gradient. The red colours in the figure on the right reflect a high catena position, while the light green colours reflect a low catenae position. Landform classes are determined using a modified (De Reu et al., 2013), multiscale (600 and 2400 m neighbourhood sizes) topographic position index algorithm first described by Weiss (2001), based on a digital elevation model (DEM), derived from the global C-band shuttle radar topographic mission (SRTM) with a 30 m resolution.

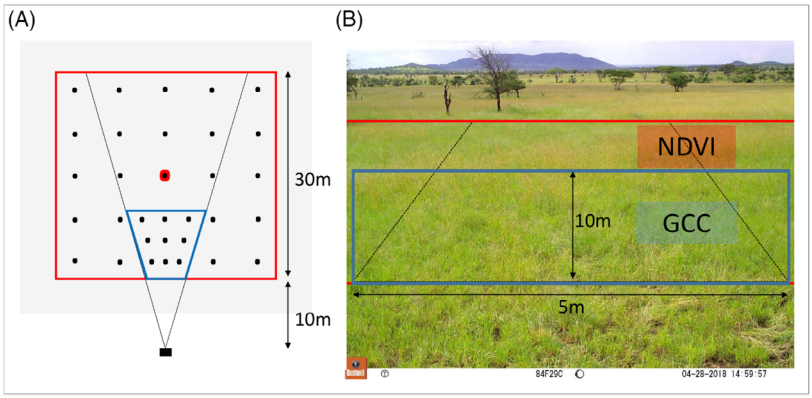

Figure 2. (A) Experimental design of the multi-scaled plot for measurement of VI's. The blue polygon indicates the ROI for extracting the GCC time series using a digital camera (camera is indicated by the black rectangular). Sentinel-2 derived NDVI (NDVIs) was extracted for the pixel (10 × 10 m resolution) covering the UTM coordinates of the red dot at the centre of the red polygon (both in left figure). The red polygon indicates the area over which NDVI may have been calculated (due to geometric inaccuracy), and the grey area denotes a buffer-zone to exclude the influence of trees and disturbance by people and vehicles. Within both polygons, we measured NDVI in the field with a radiometer (NDVIg) and aboveground standing biomass with a disc pasture meter at every subplot (black dots). (B) Sample photo of site (A), showing the field of view of the plot used for GCC extraction (blue polygon) and a partial field-of-view of the 30 x 30 m plot for NDVIs extraction. ROI, region of interest; GCC, green chromatic coordinate; NDVI, normalized difference vegetation index.

cloud-free images. The three VI's (GCC, NDVIs and NDVIg) were thus simultaneously measured through time for each site in one multi-scaled plot (Fig. 2A). We opted for NDVI over alternative VI's because of its common use and utility for a wide range of applications (Pettorelli et al., 2005). Other commonly used VI's like the Enhanced Vegetation Index (EVI) may be a good alternative in higher biomass areas (due to its compensation for the effects of NDVI saturation) but deemed unnecessary in our study sites because NDVI has a good range in low biomass areas and in such conditions does not suffer from saturation (Huete et al., 2002). Similarly, we did not correct for the effect of optical properties of the soil background because fractional vegetation cover is high in our study area.

At the largest scale, NDVIs values were calculated for the pixel (10 m resolution) covering the centre of a 30 × 30 m plot (NDVIs plot). The NDVIs plot is larger than the resolution to account for the reported geometric inaccuracy of the Sentinel-2 satellites (within 11 m for 95.5% of the tiles; Claverie et al., 2018). To exclude NDVI signals from woody components, we selected sites without trees, shrubs and saplings within and in the close vicinity of the NDVIs plot. The ~5 × 10 m plot over which we calculated GCC values (GCC plot) was nested within the NDVIs plot (Fig. 2A). NDVIg and aboveground standing biomass (from now on biomass) were measured in 32 subplots of 1 m^2 covering both the NDVIs plot (N = 25) and GCC plot (N = 9). Within-site variability was lower than between-site variability for measured VI's and biomass (Fig. S1).

While the most important green-up phase started at this location in March, we excluded this period because long periods of cloud cover prevented optical satellite sensors from acquiring cloud-free imagery, which would make it impossible to compare the performance of digital repeat photography to satellite-based methods. Spatial variation in biomass was maximized by placing cameras along the catena sequence (sometimes described as hydrologically linked hillslopes) (Fig. 1), which is associated with strong soil differentiation and thus drives a major local gradient in resource availability (Borden et al., 2020; Khomo et al., 2011). Due to increased moisture availability, biomass can accumulate faster at lower catenae positions throughout the growing season, which introduces between-site variation in biomass during our study period, independent of phenological state (Fig. S1).

Herbaceous aboveground net primary production

Herbaceous ANPP was measured using moveable exclosures following the protocol described by McNaughton et al. (1996). This method is considered the 'benchmark' in this study, and the productivity measurements made through this method thus served as the response variable. The exclosures were set up just outside the camera's view in an area representative of the region of interest (ROI). Spatial variability in species composition, biomass and NDVI is limited at this scale (Fig. S1). At the onset of each interval, we clipped an area of 50 x 50 cm outside of the exclosure ($t0$), with comparable biomass and species

composition to that inside the exclosure. After 14 days, a 50 × 50 cm plot was clipped inside the exclosure ($t1$). We set the measurement interval at 14 days to observe within-season ANPP variation while limiting the effect of clipping errors on biomass increment estimates. In one case (site I), we clipped $T1$ after 18 days due to practical issues. Clipped biomass samples were oven-dried at the Seronera research station. Average daily herbaceous ANPP was then calculated for each site and interval as:

$$\mathrm{ANPP} = \frac{\mathrm{Biomass}_{t1} - \mathrm{Biomass}_{t0}}{\mathrm{interval\ (days)}}. \quad (1)$$

Field camera time series

We used weather-proof Bushnell Trophy Cam Essential (model 119736) camera traps to collect 3-megapixel RGB photographs in JPG format every 15 min between 9.30 and 15:30 East Africa Time. Cameras were attached to trees, 3 m above ground level, to maximize herbaceous canopy view and prevent damage by rubbing large animals (buffalo, elephant). Tree branches that obstructed the camera view were trimmed. The cameras faced either north or south to minimize overexposure as a result of direct incoming sunlight. The distance between the camera and the nearest edge of the GCC plot was 10 m, resulting in a vertical downward tilt of ~17° (Fig. 2B). The GCC plot's depth was limited to 10 m because the oblique mode of camera installation decreases the herbaceous canopy view with distance and increases the contribution of non-photosynthetic elements such as flowers and seeds to GCC (Vrieling et al., 2018) (Fig. 2B). All cameras functioned as expected throughout the wet season, except for camera A, which was not operational between 26 June 2018 and 7 July 2018 due to an unknown technical issue. Camera G was not operational due to technical failure from July 2018 onwards, and a replacement was not available.

Data from camera imagery were extracted and processed using the R package *phenopix* (Filippa et al., 2016). Before processing, the images were manually filtered for wildlife presence disrupting the view on the vegetation, lens humidity caused by rainfall and over- and underexposure. While the majority of over and underexposed images were filtered out by only including images between the set times of 9.30–15:30 EAT, we additionally limited the effect of brightness on GCC by only including images with an average digital number (DN) between 80 and 220 (Sonnentag et al., 2012). We delineated the pre-defined GCC plot as the ROI in the image (blue polygon, Fig. 2). For each image, the DN of each colour layer of the RGB image (green, red and blue light in the visible spectrum: 400–700 nm) within the ROI was extracted to yield a DN triplet (R_{DN}, G_{DN}, B_{DN}), from which GCC can be calculated as follows:

$$\mathrm{GCC} = \frac{G_{\mathrm{DN}}}{R_{\mathrm{DN}} + G_{\mathrm{DN}} + B_{\mathrm{DN}}}. \quad (2)$$

GCC values were averaged for each ROI. To reduce noise caused by between-day variation in scene illumination, Sonnentag et al. (2012) suggest calculating the 90$^{\mathrm{th}}$ percentile of all averaged GCC values (GCC90) within non-overlapping 3-day windows. In this study, we tested both unsmoothed daily GCC90 values and smoothed daily GCC90 values using a moving (overlapping) 3-day window to retain high temporal resolution. While moving windows may be adequate for estimating phenologically relevant parameters such as the start or end of the season (SOS, EOS), vegetation responses to rainfall events occur at finer time scales and require temporally detailed GCC time series.

Absolute measures of GCC were not comparable in space due to differences in observation geometry and camera performance. As an alternative, we summed the number of days on which GCC90 increased for each site and productivity measurement interval because vegetation greenness and productivity were expected to vary on a daily basis due to changes in moisture availability caused by rainfall events. We calculated background variation in GCC90 during rainfall-free periods for each site so that day to day green-up is only counted when the increase is higher than the measured, site-specific standard deviation. Additionally, we considered time lags because biomass productivity was expected to lag behind greenness changes (Huxman et al., 2004). The used GCC measure (tGCC) to predict herbaceous ANPP was then calculated as follows:

$$\mathrm{tGCC}_{ij} = \sum_{t=1-l}^{14-l} \begin{cases} 1, & \text{if } \mathrm{GCC90}_{t+1} - \mathrm{GCC90}_{t} > \mathrm{SD\,GCC90}_{i} \\ 0, & \text{otherwise} \end{cases}, \quad (3)$$

where tGCC_{ij} is the GCC measure at the i_{th} site and the j_{th} measurement interval, GCC_t is the day within the measurement interval (which ranges from $t1$ to $t14$) and l is the number of 'lag' days ranging between zero and 3 days. For each tGCC_{ij}, we thus calculated four variables based on the number of lag days. We did not consider lags beyond 3 days because an increased lag period also increases the time that herbivores may eat away material from the area used for the upcoming productivity measurements through caging.

Sentinel-2 and near-surface derived NDVI time series

Available satellite imagery between April and September 2018 was downloaded from the Copernicus Open Access Hub (https://scihub.copernicus.eu/). The images are

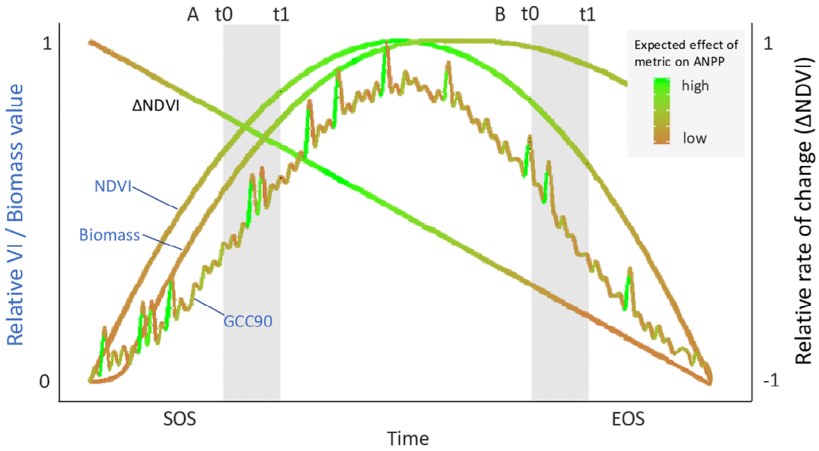

Figure 3. Overview of the expected temporal behaviour of considered predictor variables over one growing season, beginning at the SOS to the EOS. At0 – At1 and Bt0 – Bt1 represent two different productivity measurement intervals during two distinctive phenophases. The rate of change in NDVI (ΔNDVI) and disc-measured biomass are different between these two stages as NDVI generally increases during the weeks following the SOS (biomass accumulation), while NDVI decreases due to leaf senescence during the second stage of the growing season. The similar NDVI values during both A and B explains why average NDVI alone may not be informative on phenophase as both the inclusion of bare ground during early phases and leaf senescence during later phases reduces NDVI. The number of increases in GCC90 is a temporally independent predictor variable over the season. The colour gradient visualizes the expected effect of each metric (VI measures and disc-measured biomass) at different values on herbaceous ANPP without considering phenophase. SOS, start of the season; EOS, end of season; NDVI, normalized difference vegetation index; ANPP, aboveground net primary production.

acquired by two identical Sentinel-2 satellites, 2A and 2B, which each have a 10-day repeat cycle, and together provide a temporal resolution of 5 days. Before retrieving surface reflectance, we applied an atmospheric correction to all images using the Sen2cor toolbox (version 2.5.5) provided by the European Space Agency (Louis et al., 2016). Additionally, we used Sen2Cor's scene classification layer to discard pixel-level observations that were identified as clouds, cloud shadows and thin cirrus. From the 13 acquired spectral bands, we used band 4 (*R*: 0.650–0.680 nm) and 8 (NIR: 0.785–0.900 nm) at 10-m resolution to calculate NDVIs as follows (Tucker, 1979):

$$\mathrm{NDVIs} = \frac{\mathrm{NIR} - R}{\mathrm{NIR} + R}. \quad (4)$$

NDVIg was measured using a pair of two-channel (*R*: 636–673 nm, NIR: 851–879 nm) radiometric sensors (Model 1850, Skye Instruments LTD, Powys, UK). The upward-pointing sensor measures the incident solar radiation, while the second sensor measures upward reflectance from the herbaceous canopy. NDVIg is obtained from measured incoming and reflected radiation as follows:

$$\mathrm{NDVIg} = \frac{\left(\frac{\mathrm{NIR}_\rho}{\mathrm{NIR}_\sigma}\right) - \left(\frac{R_\rho}{R_\sigma}\right)}{\left(\frac{\mathrm{NIR}_\rho}{\mathrm{NIR}_\sigma}\right) + \left(\frac{R_\rho}{R_\sigma}\right)}, \quad (5)$$

where NIR and RED represent reflected quantum flux and NIR_σ and R_σ represent incident quantum flux. The radiometric sensors were mounted on top of a handheld pole at 1.5 m from the ground, which corresponds to a measured ground surface of 0.35 m^2. Every 4 days, two measurements were taken for each subplot inside the 30 × 30 m grid (N = 25) and 5 × 10 m grid (N = 9) (Fig. 2).

We calculated average NDVIs and NDVIg over the productivity measurement interval of 14 days +/− the lag days through linear interpolation (using R package *Desctools*, Signorell et al., 2016). We also considered the rate of change of both NDVI time series as they relate to phenological dynamics and phenophase (Fig. 3). Rates of change in NDVIs (ΔNDVIs) and NDVIg (ΔNDVIg) were calculated by subtracting the NDVI at the onset from the NDVI at the end of each productivity measurement. Both the start and end NDVI measurements were approximated by linear interpolation because NDVI observations do not necessarily match the onset and end of the productivity measurement interval. Positive values imply an increase in green biomass over the interval, while negative values signify senescence. Similar to tGCC, we considered different time lags for NDVIs and NDVIg.

Aboveground standing biomass

We approximated biomass at the onset of each productivity measurement using a calibrated disc-pasture meter across a 30 × 30 m grid, and a 10 × 5 m grid at each site, matching the spatial resolution of Sentinel-2 derived

Table 1. Description of predictor variables and their expected effect on herbaceous ANPP.

Predictor	Description	Predicted effect
$tGCC_x$	The number of days with increases in GCC90 (> site-specific SD) within the productivity measurement interval, with a lag of × days	Higher productivity with more days
$NDVIg_x$	Ground-based measure of NDVI averaged over the productivity measurement interval, with a lag of × days	Higher productivity with higher NDVI, which saturates or declines at the highest levels
ΔNDVIg	Ground-based NDVI at the end of each productivity measurement minus the NDVI at the onset of each productivity measurement	Higher productivity with small positive values and low productivity with negative values
$NDVIs_x$	Sentinel-2 derived measure of NDVI averaged over the productivity measurement interval, with a lag of × days	Higher productivity with higher NDVI, which saturates or declines at the highest levels
ΔNDVIs	Sentinel-2 derived NDVI at the end of each productivity measurement minus the NDVI at the onset of each productivity measurement	Higher productivity with small positive values and low productivity with negative values
Biomass	Field approximated aboveground standing biomass using a disc pasture meter at the onset of each productivity measurement interval	Increase in productivity with higher biomass, which saturates or declines at the highest levels

ANPP, aboveground net primary production; NDVI, normalized difference vegetation index.

NDVI and field camera derived GCC respectively. Disc-pasture meter measurements were averaged for each site before using a calibration equation ($R^2 = 0.83$) specific to the Serengeti to convert the height (cm) of the disc into herbaceous biomass (g m^{-2}) (unpublished data Smith et al., 2020).

Rainfall

We used the 0.05° gridded rainfall dataset from the Climate Hazards Group InfraRed Precipitation with Station data (CHIRPS) (Funk et al., 2015), downloaded from http://chg.geog.ucsb.edu/data/chirps/, to assess the responsiveness of GCC to rain events. The CHIRPS rainfall product shows consistently high performance during the entire year and for different rainfall regimes in East Africa (Kimani et al., 2017). Additionally, and recognizing that CHIRPS estimates may miss certain rain events, we also recorded rain events that could be inferred from visual examination of the camera trap images.

Data analysis

The tested predictors of herbaceous ANPP consisted of averages and rates of change in NDVIs and NDVIg, a temporal measure of GCC and disc-measured biomass (see Table 1 for an overview). Furthermore, quadratic terms for biomass, NDVIs and NDVIg were considered because herbaceous ANPP may be the highest at intermediate values of these predictors given that higher and taller biomass has increased respiratory maintenance costs due to the relatively large amounts of stem tissue and self-shading (Coughenour et al., 1984) (Fig. 3). Generalized linear models (GLM) were fit using base R and used to predict herbaceous ANPP, with quasi-Poisson distributions to correct for overdispersion (Crawley, 2012). We computed the quasi-Akaike Information Criterion (quasi-AIC) using the *bbmle* package (Bolker, 2014) for model comparison because regular AIC cannot be calculated from quasi-distributions. The least-complex model was selected when AIC was lower than 2 (Burnham and Anderson 2004).

We assessed the importance of both temporal and spatial resolution through a (stepwise) reduction of resolution in each predictor. For GCC, we reduced temporal resolution from 1 to 2 days by skipping 1 day in the dataset. This yielded two separate datasets where one GCC time series covers all the 'odd' days (starting at day 1 of the study), and the second dataset covers all the even days (starting at day 2 of the study). An increase in GCC was then calculated in a similar way as in Equation 3. We then extended the reduction in resolution up to 6 days and, as for the 2-day resolution, retained all possible x-day combinations that fitted within the time frame of 14 days. Spatial resolution was reduced from the GCC plot level (10 × 5 m, Fig. 2) to the landscape level (5 × 5 km, Fig. 1) by using the tGCC of one site (A-H) and using that value for all the other sites. This yielded eight different datasets, where the tGCC values (one for every productivity measurement interval) of one particular site were used to predict the productivity in the other sites. For biomass, temporal resolution was reduced stepwise from 2 weeks (each productivity measurement interval) to 10 weeks with steps of 2 weeks. The temporal resolution of NDVIs was reduced stepwise from 5 to 30 days with steps of 5 days. We note that a 5-day resolution is not always attained for NDVIs due to cloud cover;

Table 2. Mean aboveground standing biomass and herbaceous ANPP in the study sites for each productivity measurement interval.

Sites	Interval	*t*1	Biomass (g m^{-2})	ANPP (g m^{-2} day^{-1})
A-H	1	2018-04-30	284.78 ± 61.32	4.39 ± 3.74
	2	2018-05-14	282.03 ± 53.35	9.93 ± 8.20
	3	2018-05-28	316.38 ± 73.33	4.33 ± 4.35
	4	2018-06-11	297.67 ± 76.54	4.12 ± 3.71
	5	2018-06-25	275.21 ± 60.88	3.26 ± 3.79
	6	2018-09-02	75.07 ± 10.98	1.54 ± 1.29
I-J	1	2016-04-24	226.49 ± 163.49	5.69 ± 1.24
	2	2016-05-12	291.44 ± 220.37	0.21 ± 0.29
	3	2016-05-26	331.75 ± 260.89	0.74 ± 1.04

For both biomass and ANPP, we report the mean ± standard deviation. Biomass measurements were performed at the start of each measurement interval (*t*1) and each ANPP measurement was performed over an interval of 14 days. ANPP, aboveground net primary production.

consequently the actual temporal resolution of NDVIs can therefore be equal or greater (i.e. more days) than the assigned value in the stepwise reduction.

Finally, the dataset used for exploring the temporal responsiveness of GCC to rainfall consisted of the number of sites that recorded an increase in GCC (green-up) for each day since the last rainfall event compared to the day before the rain event occurred, for 10 separate rainfall events during the 2018 study period. To establish the effect of time since a rain event on GCC increase, we only considered rainfall events followed by at least 1 day without rain. We fitted generalized linear mixed models (GLMMs) assuming a binomial error distribution with a logit link function to model the number of sites that recorded green-up (yes or no), weighted by the total number of sites with an operational camera during the event using the *lme4* package (Bates et al., 2007). Because rain events vary in magnitude (which influences the chance that cameras may record a green-up), 'rain event ID' was included as a random effect as we were primarily interested in the effect of time in this analysis.

For the models predicting herbaceous ANPP, model fit was assessed using D^2, the proportion of deviance explained by each model relative to the null model (intercept-only model). Model consistency and predictive accuracy were evaluated using a jackknife evaluation procedure (Miller, 1974). In this procedure, one single data point (one productivity measurement at one location) is taken out of the dataset at each iteration (the number of iterations is equal to the number of data points) and predicted by a model based on the remaining data points. We report the R^2 of the regression between observed *versus* jackknife predicted values as a measure of the models' consistency. All analyses were performed in the statistical environment R version (3.4.1) (R Development Core Team 2017).

Results

Herbaceous ANPP

Herbaceous ANPP and field-measured biomass was variable between both sites and productivity measurement intervals (Table 2, Table S2). Taken over the entire study period, herbaceous ANPP was on average 4.41 g dry weight m^{-2} day^{-1} (SD = 5.02). Aboveground standing biomass was on average 261.76 g dry weight m^2 (SD = 107.07). Mean biomass was considerably lower during the 6th measurement interval of the 2018 study period because all sites burned in July 2018 (Table 2, Table S2).

Herbaceous ANPP was best predicted by a combination of tGCC, NDVIs and a quadratic term for NDVIs (ANODEV, $D^2 = 0.48$, adj. $R^2 = 0.63$) (Table 3, Fig. 4A). This result implies that both short- and long-term dynamics, as well as an indicator for biomass, are important predictors. For instance, the model predicts low herbaceous ANPP for the first 2 weeks of September 2018 compared to May 2018 (Fig. 4E and B) due to low biomass (and hence low NDVIs values) over majority of the landscape as a result of burning in July. When only ground-based methods were considered, herbaceous ANPP was predicted best by tGCC combined with a quadratic term for disc-measured biomass (ANODEV; $D^2 = 0.43$, adj. $R^2 = 0.55$, Fig. 4) (Table 3). Both of these models performed better than the best satellite-based model, where NDVIs in combination with a quadratic term for NDVIs explained 34% of deviance (ANODEV; adj. $R^2 = 0.40$). The jackknife evaluation procedure showed that the estimates of the best ground-based method (tGCC + Biomass) and best overall model (tGCC + NDVIs) were predictive of observed values (Table 3). The intercepts and slopes of the regression models between observed and jackknife predicted values were not different from 0 and 1 respectively ($P > 0.05$, Fig. S2).

We used tGCC measures calculated from unsmoothed GCC90 time series for each model because models using tGCC calculated from smoothed time series (using an overlapping 3-day window) had low quasi AIC scores and were poor predictors of herbaceous ANPP (Table S1).

Table 3. Analysis of deviance table for generalized linear models with quasi-Poisson errors considering measures of three vegetation indices (tGCC, NDVIg, NDVIs) and field-based measurements of biomass (Biomass).

	VI	Predictor	d.f.	Res. deviance	Prop. deviance	Resid d.f.	*F*	*P*	Adj R^{21}	*jk* Adj. R^{21}
tGCC		Null		265.95		49				
	tGCC	$tGCC_0$	1	211.3	0.205	48	13.28	<0.001	0.17	0.07
	tGCC + Biomass	$tGCC_3$	1	226.67	0.148	48	12.81	<0.001		0.46
		Biomass	1	176.74	0.188	47	16.28	<0.001	0.55	
		$Biomass^2$	1	152.74	0.090	46	7.830	0.007		
NDVI	$NDVIg_0$	Null		244.81		44				
		NDVIg	1	200.4	0.181	43	9.883	0.003	0.18	0.09
	$NDVIs_3$	NDVIs	1	204.18	0.166	43	11.220	0.002		0.26
		ΔNDVIs	1	202.85	0.005	42	0.368	0.548	0.40	
		$ΔNDVIs^2$	1	161.85	0.167	41	11.322	0.002		
tGCC + NDVI	$NDVIg_3$	Null		238.64		43				
		NDVIg	1	183.92	0.230	42	13.849	<0.001	0.45	0.28
		tGCC3	1	164.12	0.08	41	5.009	0.031		
	$NDVIs_2$	ΔNDVIs	1	238.43	<0.001	42	0.074	0.786	0.63	0.52
		$ΔNDVIs^2$	1	207.9	0.128	41	10.813	0.002		
		$tGCC_1$	1	136.49	0.299	40	25.285	<0.001		
		NDVIs	1	123.2	0.057	39	4.705	0.036		

We present multiple models for tGCC (based on lowest quasi-AIC scores); a model without other predictors, and models in combination with biomass, NDVIg (field-based methods) and NDVIs (satellite-based method). The adjusted R^2 of the regression between observed *versus* predicted values (Adj. R^2) and between observed *versus* jackknife predicted values (*jk* Adj. R^2) is presented for each model. The proportion deviance (prop. deviance in the table) is the proportional decrease in residual deviance relative to the null model. The ordering of predictors in the model is based on significance (*P*-value) to demonstrate the added importance (in terms of explained deviance) for each predictor.

[1]The reported adjusted R^2 is the degree to which the model predictions are correlated to observations.

Considering single VI's, we found that tGCC explained more deviation ($D^2 = 21\%$) than NDVIg ($D^2 = 18\%$) and NDVIs ($D^2 = 17\%$). Lastly, there was no consistent effect of the used lag across VI measures and different lags had little effect on the explained deviance, as indicated by low quasi AIC between models with different lags (Tables S3–S7). This implies that the potential effect of the lag in productivity after greenness changes may be very limited at the temporal scale of 3 days or that the effect is variable over time and/or between sites.

Spatiotemporal resolution of vegetation indices

The temporal profile of camera-derived GCC90 showed strong day to day fluctuation (Fig. 5). The profiles of NDVIg and NDVIs showed fewer fluctuations due to lower temporal resolution, where in some cases, the NDVIs time series was interrupted by observation gaps of up to 15 days. The importance of temporal resolution in relation to the predictive capacity of tGCC is demonstrated by a substantial decrease in the minimum adjusted R^2 (observed vs. estimated values) of both the best overall model (tGCC in combination with NDVIs and NDVIs) and the best field-based model (tGCC in combination with disc-measured biomass) with reduced temporal resolution (Fig. 6A). Similarly, a reduction in spatial resolution (from the GCC plot level to the landscape level) decreased the mean adj. R^2 of both models in a comparable way to the reduction in temporal resolution (Fig. 6B). The predictive capacity of models with a lower temporal resolution for NDVIs increased slightly at a resolution of ≥10 days (mean adj. R^2 of 0.65) before it steadily decreased (Fig. 6C). The reduction in spatial resolution for NDVIs and disc-measured biomass showed slightly smaller reductions in mean adj. R^2 compared to tGCC (Fig. 6D and F). Finally, temporal resolution was least important for disc-measured biomass, with only a minimal decrease in mean adj. R^2 (Fig. 6E).

Responsiveness of GCC to rain events

The proportion of sites that recorded a green-up in GCC was the highest on the same day as the rain event and decreased with each following day (GLMM, $z = -5.893$, $P < 0.001$) (Fig. 7). The proportions dropped steeply after the first day, except for the heavy rainfall event that occurred on the 19th of June 2018, which resulted in a green-up that was still detectable in three out of seven sites until the fifth day after the rain event (Fig. 7). GCC did not increase in response to each estimated rain event on every site.

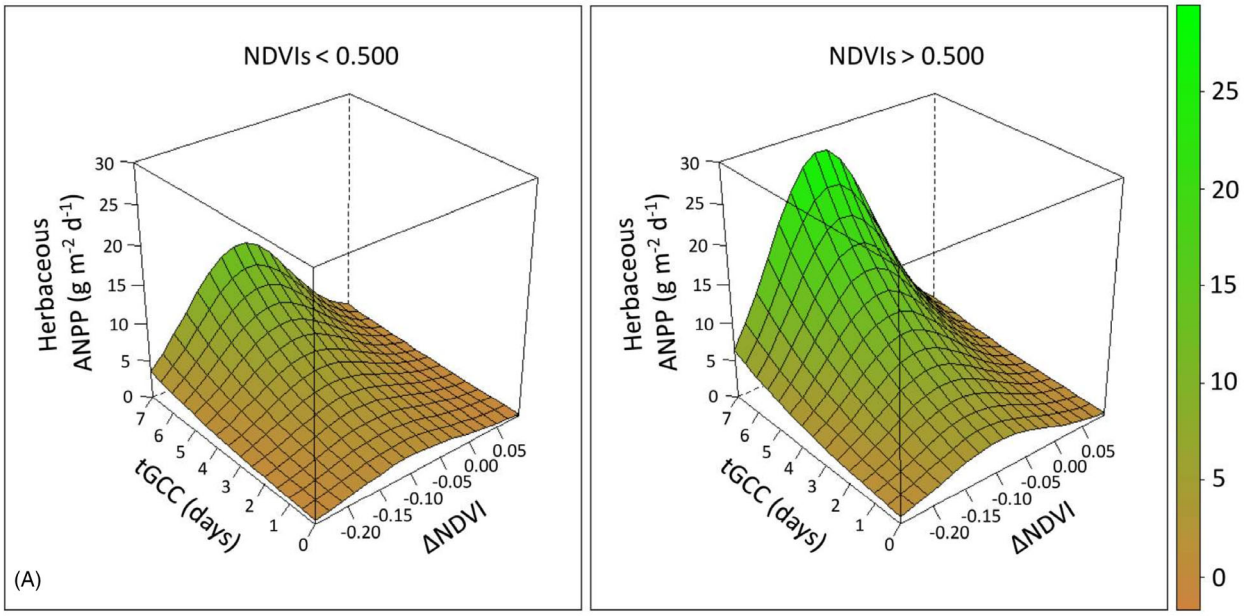

Satellite + tGCC Satellite

T1: 30-04-2018

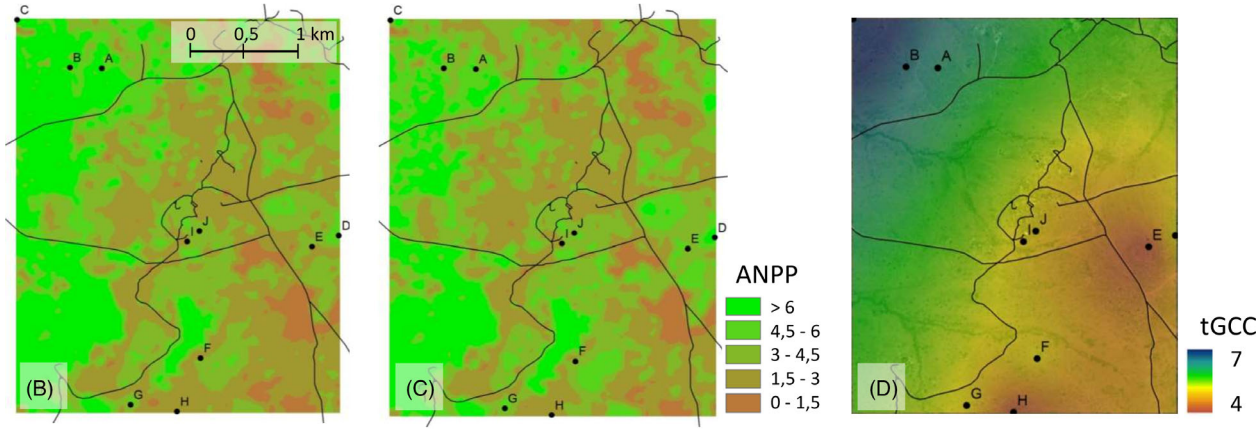

T6: 02-09-2018

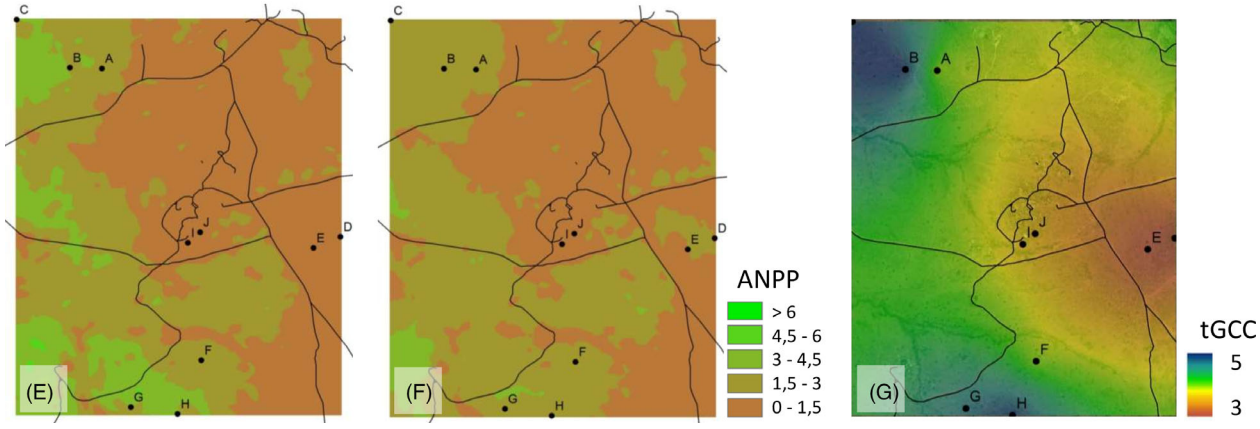

Figure 4. (A) Predicted herbaceous ANPP (grams dry weight m^{-2} day^{-1}) (*z*-axis) based upon the best model, explaining 48% of total deviance (Table 2). The model includes the number of days with measurable increases in GCC90 (tGCC, *y*-axis), a quadratic term for ΔNDVIs (*x*-axis) and a time-integrated measure of NDVIs. The effect of NDVIs is here visualized by showing the predictive behaviour of the other predictors in the model at low NDVIs (<0.500, left panel) and high NDVIs (>0.500, right panel). (B–G) Maps of the study area showing the predicted ANPP and interpolated tGCC values (obtained through ordinary kriging) for two productivity measurement intervals (*T*1 and *T*6) according to the best model combining tGCC and NDVIs (B and E) and the best satellite-based model (C and F). Note that the colour scale is different from the scale used in (A) to aid the visualization of spatial differences in productivity. ANPP, aboveground net primary production.

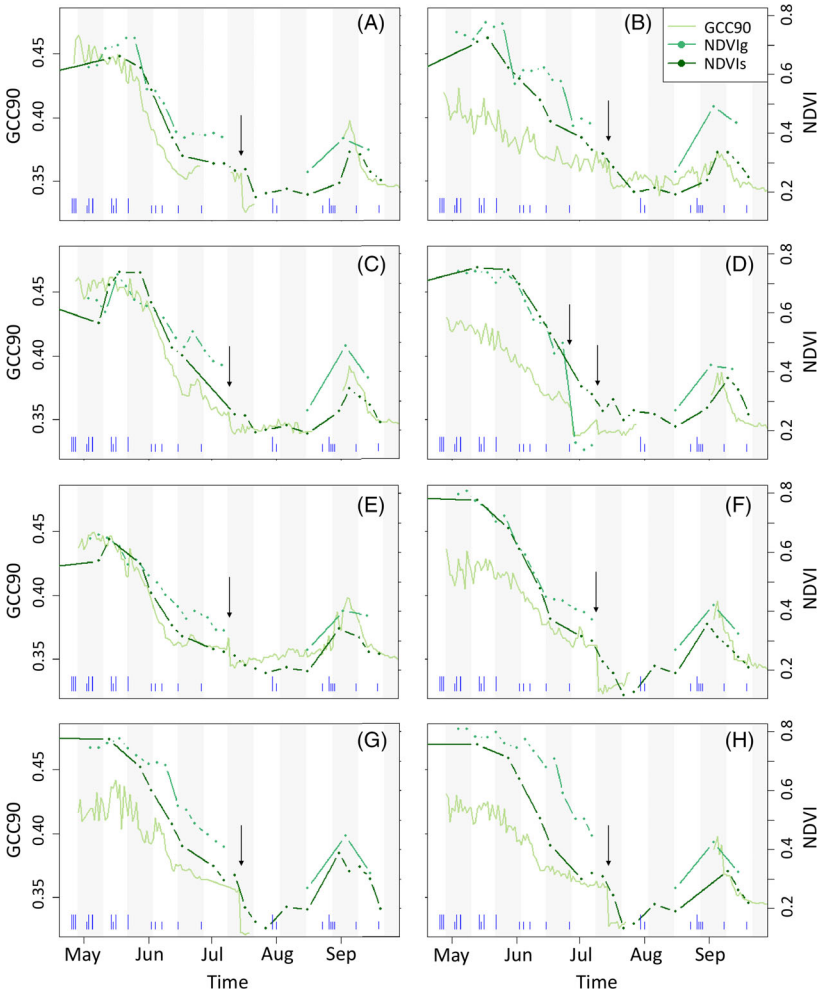

Figure 5. Time series of field camera derived GCC90 (primary *y*-axis), satellite-derived NDVI (NDVIs) and ground-based NDVI (NDVIg) (secondary *y*-axis) during the second study period (2018). Each panel is related to one site (A–H). CHIRPS-estimated precipitation events are represented as a rug (blue vertical lines) at the bottom of each panel with a distinction between small (5 mm). Arrows indicate the occurrence of a fire event. The grey shadings represent 2-week intervals. NDVI, normalized difference vegetation index; CHIRPS, Climate Hazards Group InfraRed Precipitation with Station data.

Discussion

We provided the first analysis on the capacity of camera-derived GCC to improve estimates of herbaceous ANPP relative to satellite- or ground-based NDVI measures. The results show that day-to-day increases in GCC90 are related to CHIRPS-derived rainfall events (Fig. 7) and that the sum of these daily GCC increases (tGCC) enhances the predictive capacity of both a field-based model and a remote-sensing approach (Table 3). Both models provide new herbaceous ANPP estimation methods, with reported predictive accuracy of $R^2 = 0.44$ (field-based method) and $R^2 = 0.52$ (remote-sensing approach). It should be noted that these R^2 values can be considered as high, since part of the unexplained variation results from different types of sampling errors, including clipping

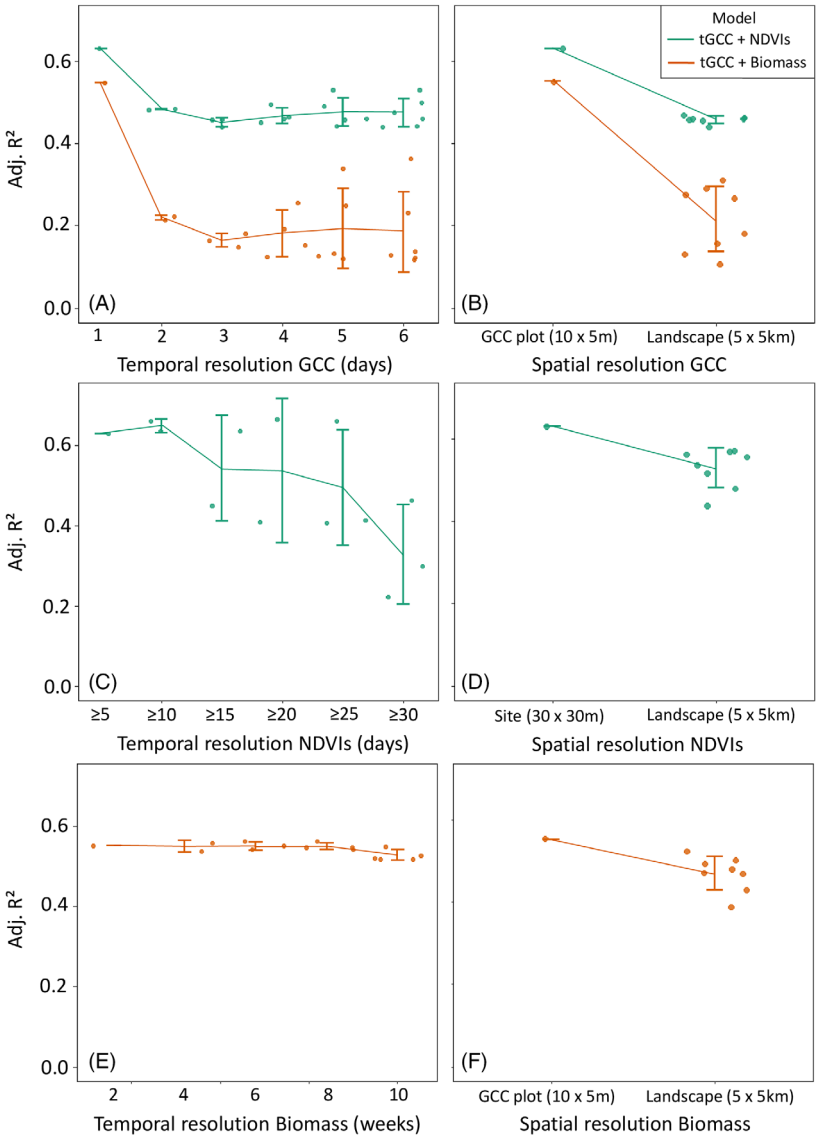

Figure 6. The effect of temporal and spatial resolution of tGCC (A and B), NDVIs (C and D) and disc-measured aboveground standing biomass (E and F) on the mean predictive capacity (given by the adjusted R^2) of the best overall model (tGCC in combination with NDVIs and ΔNDVIs) and the best field-based model (tGCC in combination with disc-measured biomass). The resolution is reduced for one predictor variable at the time. The other predictors in the model are kept constant at the highest possible resolution.

errors (e.g. judgement on the boundary of the quadrat and clipping heights between herbaceous species) (Bonham, 2013) and errors resulting from variability of biomass inside GCC plots (Fig. S1) (McNaughton et al., 1996).

The benefit of using camera-derived GCC in predicting productivity lies in the increased temporal resolution that enables cameras to detect rapid changes in vegetation greenness. While these increases could be caused by measurement errors due to variable incoming radiation between days, we are confident that the contribution of these errors has remained limited because we have both used a threshold (accounting for site-specific background variation) and applied the GCC90 calculation. The 90th percentile has been shown to effectively suppress variable scene illumination effects (Sonnentag et al., 2012). The amplitude of daily fluctuations was variable between sites (Fig. 5), which may reflect vegetation responses in absolute ways and be informative of production. However, it may also be driven by site-specific conditions such as

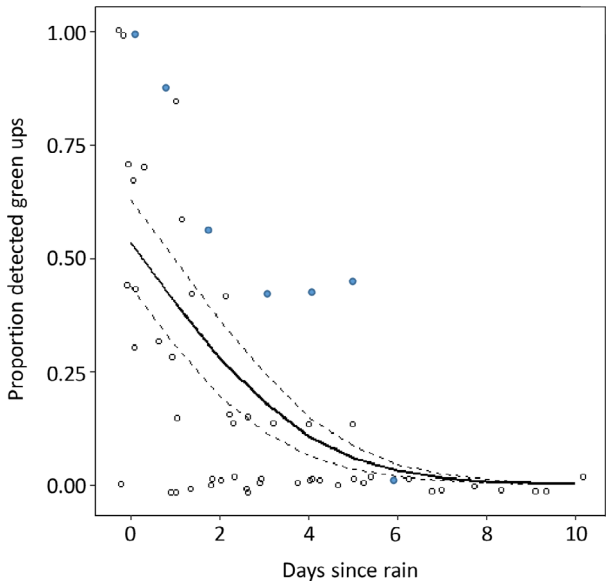

Figure 7. Predicted relationship with 95% confidence interval between the proportion of instances of daily GCC increase beyond the set threshold (> site-specific SD) and the day since last estimated rainfall event (merged information from CHIRPS and visually observed on camera trap images). The proportion is calculated as the number of sites that recorded green-up divided by the total number of sites and is given for 10 separate rainfall events during the 2018 study period. The heavy rainfall event of 19 June 2018 is indicated with blue points. Note that the data points are jittered to prevent overplotting of discrete values. CHIRPS, Climate Hazards Group InfraRed Precipitation with Station data; GCC, green chromatic coordinate.

vegetation biomass, plant species composition, herbivore pressure and camera performance. For example as herbivores are generally attracted to short-statured lawns (Hempson et al., 2015; McNaughton et al., 1997), grazers may exhaust green vegetation quicker in low biomass sites compared to high biomass sites and thereby limit measurable changes in GCC more in the former. Another possibility is that moisture-driven green-up is more easily observed in high biomass sites as more leaf material is present to respond to increased moisture availability. In this study, we accounted for site-specific background noise (by only counting a green-up when the increase in GCC90 surpassed the standard deviation in GCC90), but further investigation may be needed to understand the contribution of biomass on GCC time series behaviour. Finally, the inclusion of forbs, which have different life cycles and spectral properties than grasses (Mbow et al., 2013), could change the effect of rainfall on tGCC. In this light, caution is warranted when extrapolating tGCC over a landscape from point measurements (camera locations) (Fig. 4D and G) when the study area includes different grassland types.

The study period mainly covered the reproductive and senescence phase of herbaceous vegetation. While we find strong relationships between (combinations of) measures of VI's and herbaceous ANPP, strategies on the allocation of resources can vary between phenophases (Gu et al., 2003). Generally, the onset of flowering is associated with declines in nutrient uptake, which may make grasses relatively more water- than nutrient-limited towards the end of the growing season (Veresoglou & Fitter, 1984). A stronger link between rainfall and production during later phenophases may explain why tGCC is a good predictor of ANPP in our study. In the tropics, however, we expect the effect of phenophase to be less important as tropical savanna grasses are known to use available water as quickly as possible (Xu et al., 2015), which is thought to provide them with a competitive advantage in environments characterized by unpredictable, but heavy rainfall events (Williams et al., 1998). Nevertheless, closer investigation of the relationship between tGCC and ANPP at the start of the growing season may yield additional insights on the use of averaged and temporal measures of VI's to predict herbaceous ANPP.

Prediction of aboveground net primary productivity in natural ecosystems

All three considered VI's had limited predictive capacity of herbaceous ANPP when used alone, while combinations of tGCC with either NDVIs measures or disc-measured biomass perform well (Table 3). This implies that at least two forms of information are needed to predict herbaceous ANPP at high temporal resolution: a measure that describes vegetation state (which could be phenological or in terms of biomass) and a measure that captures vegetation responses to water inputs.

Several measures of NDVI, such as the maximum NDVI over a growing season and time-integrated NDVI, have been suggested to be good predictors of annual ANPP (Hobbs, 1995; Paruelo et al., 1997). Grassy biomes, such as grasslands and savannas, are believed to be suitable systems to derive estimates on annual ANPP from NDVI data due to the synchrony between canopy development and photosynthetic activity (Paruelo et al., 1997). At longer time scales, periods of temporary low productivity are averaged out and what remains is the gradual build-up of aboveground standing biomass in response to accumulative rainfall. We hypothesized that at shorter time scales, average NDVI would become less informative because of the alternation between productive and less productive periods during the same season due to the stochastic nature of rainfall in tropical savannas. Our study confirms that a measure that describes the change

in NDVIs over 2 weeks (ΔNDVIs) explains more variation in ANPP than average NDVIs over the same period (Table 3). NDVIs signifies increases or decreases in green biomass (Myneni et al., 1995) and consequently can provide information on the phenological state of the vegetation (Cheng et al., 2020) (Fig. 3). While further analysis may confirm or refute this, given that our model focusses on a change in NDVI and alternative vegetation indices (like EVI) represent such changes similarly, we expect that at best small improvements could arise from testing alternative spectral VIs. The fitted model predicts that productivity is lowest at the highest and the lowest (negative) values of NDVIs (Fig. 4A). High values may reflect herbaceous vegetation in a 'young' phenological stage, which occurs commonly at the SOS, after fire events, or in sites with high grazing intensity (McNaughton, 1985). Low biomass may have limited productivity in these cases (Fig. 4E and F). Negative values for NDVIs were mostly associated with the EOS, where large fractions of green biomass turned brown. Despite rainfall inputs in this period (Fig. 5), decreased photosynthetically active tissue may have limited the ability of the plants to fully respond to this input (Schwinning & Sala, 2004), which explains why late-season rainfall, in general, is a poor predictor of productivity in other C4-dominated grassy biomes (Post & Knapp, 2019).

Spatiotemporal resolution and responsiveness to rain events

The high predictive capacity of models with reduced temporal resolution (≥10 days) in NDVIs (Fig. 6C) supports the explanation that NDVIs is a good predictor of productivity because it reflects the vegetation's maturity. Phenological cycles of tropical grasses play out at the time scales of months (Parihar & Pathak, 2006). Separation of distinct phenophases, such as canopy development and canopy maturation, should therefore not require NDVI measurements at high temporal resolution. While some models still had high adj. R^2 values beyond a resolution of ≥10 days, the mean predictive capacity of models seemed to decrease. This could be explained by specific time moments that were excluded in the reduced datasets of these models; accurate prediction on the phenological state can be sensitive to observation gaps (Melaas et al., 2016), and in this study, some models at reduced resolution may have missed, or 'flattened' the peak of the season. Lastly, the poor fit of models that include ground-based NDVI measurements (Table 3) may have been caused by the high temporal resolution of NDVIg (every 4 days) (Table 3). The observed short-term increases in NDVIg may have, for example concealed the senescence phase in sites B and C (Fig. 5) and thereby have caused an overestimation in productivity during this phase.

Automated field cameras allowed us to derive GCC time series at high temporal resolution and therefore provide detailed information on productive periods. The clear responses of GCC to rainfall events (Fig. 7) support the idea that tropical savanna vegetation responds instantly to rainfall (Moreno-de las Heras et al., 2012; Schwinning & Sala, 2004; Williams et al., 1998) and that these responses can be used to predict herbaceous ANPP. The fact that vegetation sometimes failed to respond to rainfall (Fig. 7) may be because rain events were not actually measured at each camera location but relied predominantly on CHIRPS estimates. The absence of green-up could therefore have resulted from local variations in rainfall, whereby not all camera locations received the CHIRPS-estimated rainfall. Besides the temporal component, the spatial resolution of tGCC thus plays an important role as well (visualized in Fig. 4B–G), which is supported by the decrease in mean adj. R^2 of models with reduced spatial resolution in tGCC (Fig. 6B). Interestingly, two models using a tGCC measure with reduced temporal resolution (5 and 6 days) showed relatively high adj. R^2 (Fig. 6A). These models could have by 'chance' captured influential rain events (by including a GCC measurement within 1 day after a rain event) while most of the models using tGCC at the same temporal resolution (at different starting data) had no predictive capacity.

The best field-based model, which included tGCC and a quadratic term for disc-measured biomass, had slightly lower predictive capacity compared to the overall best model that combined ground-based and satellite-based methods (Table 3). The result that temporal resolution is of minimal importance for disc-measured biomass (Fig. 6E) supports the idea that the field-based model partly misses the previously mentioned phenological context as disc pasture meters cannot distinguish between green and dead biomass. In the field-based model, disc-measured biomass likely captures the effect of spatial variation in biomass (Fig. 6F) and thus the generally positive effects of biomass on herbaceous ANPP as more can be produced when there is more photosynthetic active plant material. Because the field-based model relies on methods that do not require cloud-free images, it could serve as an (temporary) alternative during periods of prolonged cloud-cover. While it is still more labour intensive than the satellite-based method, the results imply that the method only requires a single site visit in 10 weeks' time while reaching a similar accuracy.

Applications and conclusion

Accurate estimates of herbaceous ANPP serve a wide variety of ecological applications. Here, we have presented a

new method that improves the temporal resolution of such estimates. A better description of short-term productivity can help to understand and model a range of ecological processes, such as animal movement dynamics. Animal movements are generally shaped by the dynamic nature of forage resources at multiple spatial scales (Aikens et al., 2020). Migratory routes in natural grassy ecosystems function both as corridors between seasonal ranges (ecosystem scale), but are also foraging habitat themselves on local scales (Aikens et al., 2017). In these local contexts, herbivores are attracted to green pastures with high nutritional quality, but they may be limited by the available quantity (Voeten et al., 2010). Accurate productivity estimates at fine resolution could help us understand movement choices and strategies because they provide an estimate on both the resource' future quantity and quality (freshly produced pasture). Another application is to get more reliable *in situ* measurements at specific locations, which can help to improve empirical and physical of forage productivity or biomass accumulation in tropical grassy biomes.

An advantage of using field cameras to estimate ANPP is that digital repeat imagery is a ubiquitous, multipurpose tool with applications in, for example the study of phenology and the monitoring of wildlife. Phenology plays an important role in key ecosystem functions and processes such as competitive interactions, trophic dynamics, primary production and nutrient cycling (Cleland et al., 2007; Morisette et al., 2009). The use of field cameras enables researchers to characterize the entire seasonal trajectory of herbaceous canopy greenness and the spatiotemporal distribution of herbivores while at the same time having good estimates of ANPP when combined with either field-approximated biomass (in space) or satellite-derived NDVI measures.

This study highlights that the key to successfully estimating herbaceous ANPP on short time intervals is to detect the spatial and temporal variability in response to rain. By quantifying the response to rain over a time interval, camera-derived measures like tGCC offer an important contribution to both field-based methods (in the absence of cloud-free imagery) and remote-sensing approaches. While in need of further evaluation in other phenophases and ecosystems, we conclude that field cameras can offer a reliable and cost-effective method to improve the estimation of herbaceous ANPP.

Acknowledgements

We thank the management and research staff at Serengeti Wildlife Research Center, Tanzanian Wildlife Research Institute, Tanzanian National Park Authority and Tanzanian Commission for Science and Technology for their help and support while undertaking this study. Second, we thank Emilian Mayemba, Robbert van Gool, James Fredrickson, Toni Hoenders and Neha Mohan Babu for much appreciated help in the field. This study was part of the AfricanBioServices project and funded by the EU Horizon 2020 grant number 641918.

References

Aikens, E.O., Kauffman, M.J., Merkle, J.A., Dwinnell, S.P., Fralick, G.L. & Monteith, K.L. (2017) The greenscape shapes surfing of resource waves in a large migratory herbivore. *Ecology Letters*, **20**(6), 741–750. https://doi.org/10.1111/ele.12772

Aikens, E.O., Mysterud, A., Merkle, J.A., Cagnacci, F., Rivrud, I.M., Hebblewhite, M. et al. (2020) Wave-like patterns of plant phenology determine ungulate movement tactics. *Current Biology*, **30**(17), 3444–3449. https://doi.org/10.1016/j.cub.2020.06.032

Alberton, B., Torres, R.D.S., Cancian, L.F., Borges, B.D., Almeida, J., Mariano, G.C. et al. (2017) Introducing digital cameras to monitor plant phenology in the tropics: applications for conservation. *Perspectives in Ecology and Conservation*, **15**(2), 82–90. https://doi.org/10.1016/j.pecon.2017.06.004

Baret, F. & Guyot, G. (1991) Potentials and limits of vegetation indices for LAI and APAR assessment. *Remote Sensing of Environment*, **35**(2–3), 161–173. https://doi.org/10.1016/00344257(91)90009-U

Bates, D., Sarkar, D., Bates, M.D. & Matrix, L. (2007) The lme4 package. R package version, 2(1), 74. Available from: https://CRAN.R-project.org/package=lme4 [Accessed 22nd September 2019].

Bolker, B. (2014) Dealing with quasi-models in R. *Compare*, *1* (5.452).

Bonenfant, C., Gaillard, J.M., Coulson, T., Festa-Bianchet, M., Loison, A., Garel, M. et al. (2009) Empirical evidence of density-dependence in populations of large herbivores. *Advances in Ecological Research*, **41**, 313–357. https://doi.org/10.1016/S0065-2504(09)00405-X

Bonham, C.D. (2013) Biomass. In: *Measurements for terrestrial vegetation*. John Wiley & Sons, pp. 175–216. https://doi.org/10.1002/9781118534540.ch8

Borden, R.W., Baillie, I.C. & Hallett, S.H. (2020) The East African contribution to the formalisation of the soil catena concept. *Catena*, **185**, 104291. https://doi.org/10.1016/j.catena.2019.104291

Brun, P., Zimmermann, N.E., Graham, C.H., Lavergne, S., Pellissier, L., Münkemüller, T. et al. (2019) The productivity-biodiversity relationship varies across diversity dimensions. *Nature Communications*, **10**(1), 1–11. https://doi.org/10.1038/s41467-019-13678-1

Burnham, K.P. & Anderson, D.R. (2004) Multimodel inference: understanding AIC and BIC in model selection. *Sociological methods & research*, **33**(2), 261–304.

Byrne, K.M., Lauenroth, W.K., Adler, P.B. & Byrne, C.M. (2011) Estimating aboveground net primary production in grasslands: a comparison of nondestructive methods. *Rangeland Ecology & Management*, **64**(5), 498–505. https://doi.org/10.2111/REM-D-10-00145.1

Cebrian, J. (1999) Patterns in the fate of production in plant communities. *The American Naturalist*, **154**(4), 449–468. https://doi.org/10.1086/303244

Cheng, Y., Vrieling, A., Fava, F., Meroni, M., Marshall, M. & Gachoki, S. (2020) Phenology of short vegetation cycles in a Kenyan rangeland from planet scope and Sentinel-2. *Remote Sensing of Environment*, **248**, 112004. https://doi.org/10.1016/j.rse.2020.112004

Claverie, M., Ju, J., Masek, J.G., Dungan, J.L., Vermote, E.F., Roger, J.C. et al. (2018) The harmonized Landsat and Sentinel-2 surface reflectance data set. *Remote Sensing of Environment*, **219**, 145–161. https://doi.org/10.1016/j.rse.2018.09.002

Cleland, E.E., Chuine, I., Menzel, A., Mooney, H.A. & Schwartz, M.D. (2007) Shifting plant phenology in response to global change. *Trends in Ecology & Evolution*, **22**(7), 357–365. https://doi.org/10.1016/j.tree.2007.04.003

Coughenour, M.B., McNaughton, S.J. & Wallace, L.L. (1984) Modelling primary production of perennial graminoids uniting physiological processes and morphometric traits. *Ecological Modelling*, **23**(1–2), 101–134. https://doi.org/10.1016/0304-3800(84)90121-2

Crawley, M.J. (2012) The R book. *John Wiley & Sons.* https://doi.org/10.1002/9781118448908

De Reu, J., Bourgeois, J., Bats, M., Zwertvaegher, A., Gelorini, V., De Smedt, P. et al. (2013) Application of the topographic position index to heterogeneous landscapes. *Geomorphology*, **186**, 39–49. https://doi.org/10.1016/j.geomorph.2012.12.015

Filippa, G., Cremonese, E., Migliavacca, M., Galvagno, M., Forkel, M., Wingate, L. et al. (2016) Phenopix: AR package for image-based vegetation phenology. *Agricultural and Forest Meteorology*, **220**, 141–150. https://doi.org/10.1016/j.agrformet.2016.01.006

Frank, D.A. & McNaughton, S.J. (1993) Evidence for the promotion of aboveground grassland production by native large herbivores in Yellowstone National Park. *Oecologia*, **96**(2), 157–161. https://doi.org/10.1007/BF00317727

Funk, C., Peterson, P., Landsfeld, M., Pedreros, D., Verdin, J., Shukla, S. et al. (2015) The climate hazards infrared precipitation with stations—a new environmental record for monitoring extremes. *Scientific Data*, **2**(1), 1–21. https://doi.org/10.1038/sdata.2015.66

Gu, L., Post, W.M., Baldocchi, D., Black, T.A., Verma, S.B., Vesala, T. et al. (2003) Phenology of vegetation photosynthesis. In: Schwartz, M.D. (Ed.) *Phenology: an integrative environmental science*. Springer, pp. 467–485. https://doi.org/10.1007/978-94-007-0632-3_29

Hempson, G.P., Archibald, S., Bond, W.J., Ellis, R.P., Grant, C.C., Kruger, F.J. et al. (2015) Ecology of grazing lawns in Africa. *Biological Reviews*, **90**(3), 979–994. https://doi.org/10.1111/brv.12145

Hobbs, T.J. (1995) The use of NOAA-AVHRR NDVI data to assess herbage production in the arid rangelands of Central Australia. *International Journal of Remote Sensing*, **16**(7), 1289–1302. https://doi.org/10.1080/01431169508954477

Huete, A., Didan, K., Miura, T., Rodriguez, E.P., Gao, X. & Ferreira, L.G. (2002) Overview of the radiometric and biophysical performance of the MODIS vegetation indices. *Remote Sensing of Environment*, **83**(1–2), 195–213. https://doi.org/10.1016/S0034-4257(02)00096-2

Huete, A.R., Jackson, R.D. & Post, D.F. (1985) Spectral response of a plant canopy with different soil backgrounds. *Remote Sensing of Environment*, **17**(1), 37–53. https://doi.org/10.1016/0034-4257(85)90111-7

Huxman, T.E., Snyder, K.A., Tissue, D., Leffler, A.J., Ogle, K., Pockman, W.T. et al. (2004) Precipitation pulses and carbon fluxes in semiarid and arid ecosystems. *Oecologia*, **141**(2), 254–268. https://doi.org/10.1007/s00442-004-1682-4

Jager, T. (1982) *Soils of the Serengeti woodlands, Tanzania*. Wageningen, the Netherlands: Centre for Agricultural Publishing and Documentation (Pudoc).

Khomo, L., Hartshorn, A.S., Rogers, K.H. & Chadwick, O.A. (2011) Impact of rainfall and topography on the distribution of clays and major cations in granitic catenas of southern Africa. *Catena*, **87**(1), 119–128. https://doi.org/10.1016/j.catena.2011.05.017

Kimani, M.W., Hoedjes, J.C. & Su, Z. (2017) An assessment of satellite-derived rainfall products relative to ground observations over East Africa. *Remote Sensing*, **9**(5), 430. https://doi.org/10.3390/rs9050430

Louis, J., Debaecker, V., Pflug, B., Main-Knorn, M., Bieniarz, J., Mueller-Wilm, U. et al. (2016) Sentinel-2 Sen2Cor: L2A processor for users. In *Proceedings living planet symposium 2016*, pp. 1–8. Spacebooks Online.

Mbow, C., Fensholt, R., Rasmussen, K. & Diop, D. (2013) Can vegetation productivity be derived from greenness in a semi-arid environment? Evidence from ground-based measurements. *Journal of Arid Environments*, **97**, 56–65. https://doi.org/10.1016/j.jaridenv.2013.05.011

McNaughton, S.J. (1985) Ecology of a grazing ecosystem: the Serengeti. *Ecological Monographs*, **55**(3), 259–294. https://doi.org/10.2307/1942578

McNaughton, S.J., Banyikwa, F.F. & McNaughton, M.M. (1997) Promotion of the cycling of diet-enhancing nutrients by African grazers. *Science*, **278**(5344), 1798–1800. https://doi.org/10.1126/science.278.5344.1798

McNaughton, S.J., Milchunas, D.G. & Frank, D.A. (1996) How can net primary productivity be measured in grazing ecosystems? *Ecology*, **77**(3), 974–977. https://doi.org/10.2307/2265518

McNaughton, S.J., Oesterheld, M., Frank, D.A. & Williams, K.J. (1989) Ecosystem-level patterns of primary productivity and herbivory in terrestrial habitats. *Nature*, **341**(6238), 142–144. https://doi.org/10.1038/341142a0

Melaas, E.K., Sulla-Menashe, D., Gray, J.M., Black, T.A., Morin, T.H., Richardson, A.D. et al. (2016) Multisite analysis of land surface phenology in north American temperate and boreal deciduous forests from Landsat. *Remote Sensing of Environment*, **186**, 452–464. https://doi.org/10.1016/j.rse.2016.09.014

Miller, R.G. (1974) The jackknife-a review. *Biometrika*, **61**(1), 1–15. https://doi.org/10.1093/biomet/61.1.1

Moreno-de las Heras, M., Saco, P.M., Willgoose, G.R. & Tongway, D.J. (2012) Variations in hydrological connectivity of Australian semiarid landscapes indicate abrupt changes in rainfall-use efficiency of vegetation. *Journal of Geophysical Research: Biogeosciences*, **117**(G3). https://doi.org/10.1029/2011JG001839

Morisette, J.T., Richardson, A.D., Knapp, A.K., Fisher, J.I., Graham, E.A., Abatzoglou, J. et al. (2009) Tracking the rhythm of the seasons in the face of global change: phenological research in the 21st century. *Frontiers in Ecology and the Environment*, **7**(5), 253–260. https://doi.org/10.1890/070217

Myneni, R.B., Hall, F.G., Sellers, P.J. & Marshak, A.L. (1995) The interpretation of spectral vegetation indexes. *IEEE Transactions on Geoscience and Remote Sensing*, **33**(2), 481–486. https://doi.org/10.1109/TGRS.1995.8746029

Parihar, S.S. & Pathak, P.S. (2006) Flowering phenology and seed biology of selected tropical perennial grasses. *Tropical Ecology*, **47**(1), 81–88.

Paruelo, J.M., Epstein, H.E., Lauenroth, W.K. & Burke, I.C. (1997) ANPP estimates from NDVI for the central grassland region of the United States. *Ecology*, **78**(3), 953–958. https://doi.org/10.1890/0012-9658(1997)078[0953:AEFNFT]2.0.CO;2

Pellew, R.A.P. (1983) The impacts of elephant, giraffe and fire upon the *Acacia tortilis* woodlands of the Serengeti. *African Journal of Ecology*, **21**(1), 41–74. https://doi.org/10.1111/j.1365-2028.1983.tb00311.x

Pettorelli, N., Ryan, S., Mueller, T., Bunnefeld, N., Jędrzejewska, B., Lima, M. et al. (2011) The normalized difference vegetation index (NDVI): unforeseen successes in animal ecology. *Climate Research*, **46**(1), 15–27. https://doi.org/10.3354/cr00936

Pettorelli, N., Vik, J.O., Mysterud, A., Gaillard, J.M., Tucker, C.J. & Stenseth, N.C. (2005) Using the satellite-derived NDVI to assess ecological responses to environmental change. *Trends in Ecology & Evolution*, **20**(9), 503–510. https://doi.org/10.1016/j.tree.2005.05.011

Post, A.K. & Knapp, A.K. (2019) Plant growth and aboveground production respond differently to late-season deluges in a semi-arid grassland. *Oecologia*, **191**(3), 673–683. https://doi.org/10.1007/s00442-019-04515-9

R Development Core, T. (2017). A language and environment for statistical computing. Vienna: R Found. Stat. Comput..

Reid, W.V., Mooney, H.A., Capistrano, D., Carpenter, S.R., Chopra, K., Cropper, A. et al. (2006) Nature: the many benefits of ecosystem services. *Nature*, **443**(7113), 749. https://doi.org/10.1038/443749a

Richardson, A.D. (2019) Tracking seasonal rhythms of plants in diverse ecosystems with digital camera imagery. *New Phytologist*, **222**(4), 1742–1750. https://doi.org/10.1111/nph.15591

Richardson, A.D., Keenan, T.F., Migliavacca, M., Ryu, Y., Sonnentag, O. & Toomey, M. (2013) Climate change, phenology, and phenological control of vegetation feedbacks to the climate system. *Agricultural and Forest Meteorology*, **169**, 156–173. https://doi.org/10.1016/j.agrformet.2012.09.012

Ruppert, J.C. & Linstädter, A. (2014) Convergence between ANPP estimation methods in grasslands—a practical solution to the comparability dilemma. *Ecological Indicators*, **36**, 524–531. https://doi.org/10.1016/j.ecolind.2013.09.008

Sala, O.E. & Austin, A.T. (2000) Methods of estimating aboveground net primary productivity. In: Sala, O.E., Jackson, R.B., Mooney, H.A. & Howarth, R.W. (Eds.) *Methods in ecosystem science*. Springer, pp. 31–43. https://doi.org/10.1007/978-1-4612-1224-9_3

Schwinning, S. & Sala, O.E. (2004) Hierarchy of responses to resource pulses in arid and semi-arid ecosystems. *Oecologia*, **141**(2), 211–220. https://doi.org/10.1007/s00442-004-1520-8

Scurlock, J.M., Johnson, K. & Olson, R.J. (2002) Estimating net primary productivity from grassland biomass dynamics measurements. *Global Change Biology*, **8**(8), 736–753. https://doi.org/10.1046/j.1365-2486.2002.00512.x

Signorell, A., Aho, K., Alfons, A., Anderegg, N., Aragon, T. & Arppe, A. (2016) DescTools: tools for descriptive statistics. R package version 0.99-18. R Foundation for Statistical Computing, Vienna, Austria. Available from: https://CRAN.R-project.org/package=DescTools [Accessed 22nd September 2019].

Sinclair, A.R.E., Hopcraft, J.G.C., Olff, H., Mduma, S.A., Galvin, K.A. & Sharam, G.J. (2008) Historical and future changes to the Serengeti ecosystem. In: Sinclair, A.R.E., Packer, C. & Mduma, S.A.R. (Eds.) *Serengeti III: human impacts on ecosystem dynamics*. University of Chicago Press, pp. 7–46. https://doi.org/10.7208/chicago/9780226760353.001.0001

Smith, S.W., Graae, B.J., Bukombe, J., Hassan, S.N., Lyamuya, R.D., Jacob Mtweve, P. et al. (2020) Savannah trees buffer herbaceous plant biomass against wild and domestic herbivores. *Applied Vegetation Science*, **23**(2), 185–196. https://doi.org/10.1111/avsc.12472

Sonnentag, O., Hufkens, K., Teshera-Sterne, C., Young, A.M., Friedl, M., Braswell, B.H. et al. (2012) Digital repeat photography for phenological research in forest ecosystems. *Agricultural and Forest Meteorology*, **152**, 159–177. https://doi.org/10.1016/j.agrformet.2011.09.009

Toomey, M., Friedl, M.A., Frolking, S., Hufkens, K., Klosterman, S., Sonnentag, O. et al. (2015) Greenness indices from digital cameras predict the timing and seasonal dynamics of canopy-scale photosynthesis. *Ecological Applications*, **25**(1), 99–115. https://doi.org/10.1890/14-0005.1

Tucker, C.J. (1979) Red and photographic infrared linear combinations for monitoring vegetation. *Remote Sensing of Environment*, **8**(2), 127–150. https://doi.org/10.1016/0034-4257(79)90013-0

Veresoglou, D.S. & Fitter, A.H. (1984) Spatial and temporal patterns of growth and nutrient uptake of five co-existing grasses. *Journal of Ecology*, **72**(1), 259–272. https://doi.org/10.2307/2260018

Voeten, M.M., Van De Vijver, C.A., Olff, H. & Van Langevelde, F. (2010) Possible causes of decreasing migratory ungulate populations in an east African savannah after restrictions in their seasonal movements. *African Journal of Ecology*, **48**(1), 169–179. https://doi.org/10.1111/j.1365-2028.2009.01098.x

Vrieling, A., Meroni, M., Darvishzadeh, R., Skidmore, A.K., Wang, T., Zurita-Milla, R. et al. (2018) Vegetation phenology from Sentinel-2 and field cameras for a Dutch barrier Island. *Remote Sensing of Environment*, **215**, 517–529. https://doi.org/10.1016/j.rse.2018.03.014

Weiss, A.D. (2001) Topographic position and landforms analysis. Poster presentation, ESRI user conference, San Diego, CA (Vol. 200).

Williams, K.J., Wilsey, B.J., McNaughton, S.J. & Banyikwa, F.F. (1998) Temporally variable rainfall does not limit yields of Serengeti grasses. *Oikos*, **81**, 463–470. https://doi.org/10.2307/3546768

Xu, X., Medvigy, D. & Rodriguez-Iturbe, I. (2015) Relation between rainfall intensity and savanna tree abundance explained by water use strategies. *Proceedings of the National Academy of Sciences of the United States of America*, **112**(42), 12992–12996. https://doi.org/10.1073/pnas.1517382112

Supporting Information

Additional supporting information may be found online in the Supporting Information section at the end of the article.

Table S1. Universal Transverse Mercator (UTM) coordinates of study sites.

Table S2. Mean aboveground standing biomass and herbaceous ANPP in each study site (A–H for the 2018 study period and I–J for the 2016 study period) for each productivity measurement interval.

Table S3. Model fits (quasi AIC, the Akaike information criterion for generalized linear models with quasi-Poisson errors) for Herbaceous Aboveground Net Primary Productivity, considering different lags of tGCC measures (tGCCm: moving window approach) and aboveground standing biomass (Biomass).

Table S4. Model fits (quasi AIC, the Akaike information criterion for generalized linear models with quasi-Poisson errors) for Herbaceous Aboveground Net Primary productivity, considering different lags of both temporal and time-integrated measures of near-surface NDVI (NDVIg).

Table S5. Model fits (quasi AIC, the Akaike information criterion for generalized linear models with quasi-Poisson errors) for Herbaceous Aboveground Net Primary productivity, considering different lags of both temporal and time-integrated measures of sentinel derived NDVI (NDVIs).

Table S6. Model fits (quasi AIC, the Akaike information criterion for generalized linear models with quasi-Poisson errors) for Herbaceous Aboveground Net Primary productivity, considering temporal and time-integrated measures of near-surface NDVI (NDVIg), in combination with tGCC.

Table S7. Model fits (quasi AIC, the Akaike information criterion for generalized linear models with quasi-Poisson errors) for Herbaceous Aboveground Net Primary productivity, considering temporal and time-integrated measures of sentinel derived NDVI (NDVIs), in combination with tGCC.

Figure S1. Near-surface NDVIg measurements (A) and biomass (disc pasture meter) measurements (B) for sites A–H for the 3rd of May 2018 (peak of season) across multiple scales: Sentinel plot (30 x 30 m), GGC plot (10 x 5 m), and the measurement near the cage (1 x 1 m).

Figure S2. Observed versus Jackknife predicted regression plots for the best model, combining tGCC, NDVIs, and a quadratic term for NDVIs (A) and the best field-based model, combing tGCC and a quadratic term for aboveground standing biomass (B). The regression model and parameters are shown in the graph.